

Article

Radiation Response Properties of Tb-Doped MgGa_2O_4 Single Crystals

Yuma Takebuchi ¹, Satoshi Honjo ², Kazumitsu Naoe ², Takumi Kato ¹, Daisuke Nakauchi ¹,
Noriaki Kawaguchi ¹ and Takayuki Yanagida ^{1,*}

¹ Division of Materials Science, Nara Institute of Science and Technology (NAIST), Ikoma 630-0192, Japan

² Department of Chemical Engineering, National Institute of Technology, Nara College, Nara 639-1080, Japan

* Correspondence: t-yanagida@ms.naist.jp

Abstract: Tb-doped MgGa_2O_4 single crystals (0.3, 1, 3, and 5%) were synthesized by the floating zone method. The synthesized crystals had a single phase of MgGa_2O_4 confirmed by X-ray diffraction and high transparency in the visible wavelength. Tb^{3+} acted as a luminescence center in both photoluminescence (PL) and thermally stimulated luminescence (TSL) processes. In the TSL dose response functions, the minimum detectable dose of the crystals was 0.01 mGy, which was comparable with some commercial dosimetric materials. In the X-ray imaging test taken based on TSL, the spatial resolution of the 1% Tb-doped crystal was estimated to be 8.90 LP/mm (56.2 μm).

Keywords: radiation detection; dosimetry; single crystal; antisite defect



Citation: Takebuchi, Y.; Honjo, S.; Naoe, K.; Kato, T.; Nakauchi, D.; Kawaguchi, N.; Yanagida, T. Radiation Response Properties of Tb-Doped MgGa_2O_4 Single Crystals. *Crystals* **2022**, *12*, 1620. <https://doi.org/10.3390/cryst12111620>

Academic Editor: Evgeniy N. Mokhov

Received: 22 October 2022

Accepted: 10 November 2022

Published: 12 November 2022

Publisher's Note: MDPI stays neutral with regard to jurisdictional claims in published maps and institutional affiliations.



Copyright: © 2022 by the authors. Licensee MDPI, Basel, Switzerland. This article is an open access article distributed under the terms and conditions of the Creative Commons Attribution (CC BY) license (<https://creativecommons.org/licenses/by/4.0/>).

1. Introduction

Dosimetric materials are a kind of phosphors for ionizing radiation detection, which have the function of storing absorbed radiation energy via the carrier trapping phenomenon. When ionizing radiation is absorbed by dosimetric material, numerous electrons and holes (carriers) are generated. The carriers are temporally stored at trapping centers and have a metastable state. Then, they are released by receiving external stimulation, for example, heat or light. After the re-excitation of carriers from trapped states, they recombine at the luminescence center with emitting photons; the emission due to heat or light stimulation is called thermally or optically stimulated luminescence (TSL or OSL), respectively [1]. Because the luminescence intensity is proportional to the absorbed dose, TSL and OSL can derive the total amount and distribution of the absorbed dose and are applied to a wide range of applications, including personal and environmental dosimetry [2], radiation therapy [3,4], and medical imaging [5]. The main required properties for dosimetric materials are high luminescence intensity, low fading, high thermal and chemical stability, and wide dynamic range. Until now, many dosimetric materials such as C-doped Al_2O_3 [6], Tb-doped Mg_2SiO_4 [7], Cu-doped $\text{Li}_2\text{B}_4\text{O}_7$ [2], Tm-doped CaF_2 [8], and Eu-doped BaFBr [9] have been investigated and commercialized. However, no dosimetric material meets all of the above requirements; therefore, there is still a need to develop novel and effective dosimetric materials.

Although many dosimetric materials have been developed as opaque ceramics or powder form [5,10–14], a single crystal is advantageous in terms of luminescence intensity. A single crystal has higher transparency than ceramics or powder, and emitted photons can be obtained from not only the surface but also from inside the material. Therefore, more luminescence can reach a readout photodetector. On the other hand, fewer defects can be a disadvantage since it means a lower concentration of trapping centers. To use the advantage and solve the disadvantage, spinel-type crystalline materials are attractive. Spinel-type materials, which have a chemical formula of AB_2O_4 , are basically composed of tetrahedral A^{2+} ions and octahedral B^{3+} ions. However, a part of A^{2+} and B^{3+} ions are

swapped due to cation inversion, and intrinsic antisite defects are generated [15–18]. The antisite defects are useful for trapping centers, and AB_2O_4 single crystals are expected to have both high transparency and high concentration of trapping centers. Up to now, we have reported that some $MgAl_2O_4$ single crystals doped with rare earths, including Tb, showed good dosimetric properties [19–22]. Analogically, $MgGa_2O_4$, which also has a spinel-type structure, may also exhibit good dosimetric properties. Additionally, in radiation-induced luminescence, luminescence efficiency is inversely proportional to the band gap energy (E_g) of the host material [23]. Therefore, $MgGa_2O_4$ ($E_g = 4.9$ eV), which has smaller E_g than $MgAl_2O_4$ ($E_g = 7.8$ eV), is expected to have higher luminescence efficiency than $MgAl_2O_4$ in terms of E_g [24,25]. However, as far as we know, the dosimetric properties of $MgGa_2O_4$ have been investigated only in ceramic form, and research into their dosimetric properties has been limited to a few studies, such as TSL glow curves at certain doses [26,27]. In this study, we synthesized $MgGa_2O_4$ single crystals doped with various concentrations of Tb and investigated the photoluminescence and dosimetric properties.

2. Experimental Methods

Tb-doped $MgGa_2O_4$ single crystals were synthesized by the floating zone (FZ) method. The raw materials were MgO (4N, High Purity Chemicals, Saitama, Japan), Ga_2O_3 (4N, Furuuchi Chemical, Tokyo, Japan), and Tb_4O_7 (4N, Furuuchi Chemical, Tokyo, Japan) powders. Tb concentrations were 0.3, 1, 3, and 5% in molar ratios. To compensate for the evaporation of Ga_2O_3 , 30% excess Ga_2O_3 was added. This experimental condition was tested by different excess amounts of Ga_2O_3 from 5 to 40%. The crystals were grown in air atmosphere by using FZ furnace (Canon Machinery Inc., FZD0192, Shiga, Japan) under conditions of 5 mm/h and 10 rpm for pull-down and rotation rate, respectively. Other operations were performed according to a previous study [28].

A part of obtained crystalline rod was cut and polished for measurement. The portions with few cracks were selected by visual inspection and cut manually. A polishing machine (Buehler, MetaServ 250, Lake Bluff, USA) was used for mechanical polishing. Other remaining parts were crushed into powder for X-ray diffraction (XRD) measurement. An X-ray diffractometer (Rigaku, MiniFlex600, Tokyo, Japan) was used to analyze the XRD patterns. A spectrophotometer (Shimadzu, SolidSpec-3700, Kyoto, Japan) was utilized for diffuse transmittance spectrum measurements.

The PL excitation and emission spectra were investigated by a spectrofluorometer (JASCO, FP-8600, Tokyo, Japan), and PL quantum yields were acquired using Quantaaurus-QY (Hamamatsu Photonics, C11347, Shizuoka, Japan). The shortest excitation wavelength of Quantaaurus-QY was 250 nm. The PL decay curves, as well as decay time constants, were evaluated by Quantaaurus- τ (Hamamatsu Photonics, C11367, Shizuoka, Japan).

In this study, TSL properties were measured as dosimetric properties. As a radiation source, an X-ray generator (Spellman, XRB80P&N200X4550, Hauppauge, USA) was utilized. The measurements were taken immediately after irradiation. The TSL glow curves were studied by a TSL reader (NanoGray Inc., TL-2000, Osaka, Japan) at 1 °C/s in the temperature range of 50–490 °C [29]. The TSL reader was equipped with an optical shortcut filter that cuts photons longer than 520 nm to eliminate signals due to thermal radiation. TSL spectra were measured by using a CCD-based spectrometer (Ocean Optics, QE Pro, Orland, USA) under heating by an electric heater (Sakaguchi E.H Voc, SCR-SHQ-A, Tokyo, Japan) [30]. The TSL dose response functions were obtained from the peak height at 90 °C of the TSL glow curves at each irradiation dose. The irradiation dose range was from 0.01 mGy to 1 Gy, which was calibrated by ionization chamber.

The X-ray imaging test was carried out by our original setup [31]. Pb-based square wave chart (DIAGNOMATIC, Pro-Res RF BarType7, Okszow, Poland) was used as an imaging object. The tested line patterns were 4.50, 6.30, and 8.90 LP/mm (spatial resolution of 111.1, 79.3, and 56.2 μm , respectively). The crystals were irradiated by 10 Gy X-ray through the imaging object and then heated on hot plate (As One, CHO-170AF, Osaka, Japan) at approximately 300 $^{\circ}\text{C}$. The emission was read by a CCD camera (Bitran Corp., BK-54DUV, Saitama, Japan) located 40 cm away from the heater and the sample.

3. Results and Discussion

Figure 1 shows the photograph of the crystals under room light (bottom) and 254 nm UV light (top). All the crystals were visibly transparent and colorless, although some small cracks were observed. Under 254 nm UV light, all the crystals exhibited green luminescence. Figure 2 depicts the XRD patterns of the crystals. The diffraction patterns of all the crystals corresponded to the reference pattern of MgGa_2O_4 (COD 9006817) and indicated that obtained crystals had a single phase of MgGa_2O_4 . Since no peak shift was observed within the accuracy of our XRD apparatus, Tb would be doped into interstitial [32].

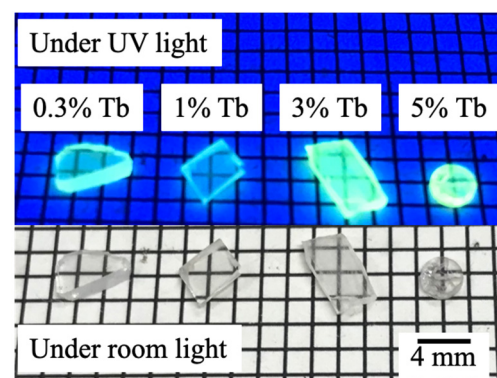


Figure 1. Photograph of the crystals under room light (bottom) and UV light (top).

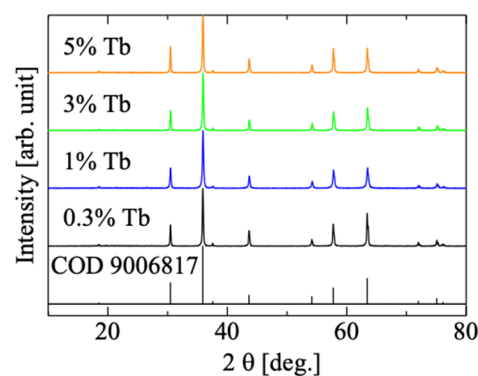


Figure 2. XRD patterns of synthesized Tb-doped MgGa_2O_4 and reference (COD 9006817).

Figure 3 displays the diffuse transmittance spectra of the crystals. All the crystals showed absorption at a wavelength shorter than 250 nm and a high transmittance of approximately 80% in the range of 300 to 850 nm. The variation in the transmittance in each crystal may be due to cracks inside the crystals. Absorption at wavelengths shorter than 250 nm was considered due to the overlap of the band gap of the host material and 4f-5d transitions of Tb^{3+} [24,33–37].

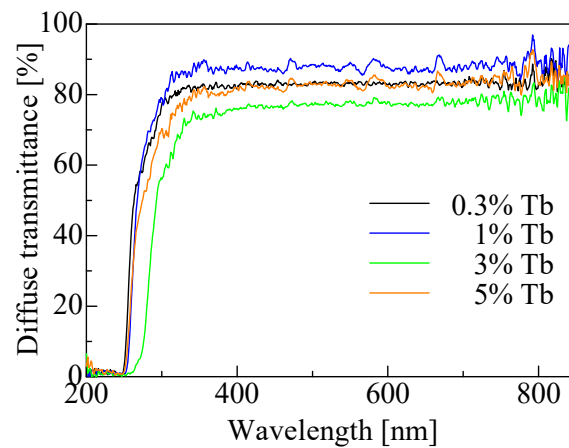


Figure 3. Diffuse transmittance spectra of Tb-doped MgGa_2O_4 .

Figure 4 presents the PL excitation (dashed line) and emission (solid line) spectra of the crystals. When the monitoring wavelength was set to 550 nm, an excitation peak was observed at around 230 nm. Since the wavelength of the excitation peak was shorter than the absorption edge observed in Figure 3, the excitation peak might be independent of the absorption edge. Referring to previous studies, the origin of the excitation peak was ascribed to the 4f-5d transitions of Tb^{3+} [35–37]. Under excitation at 230 nm, all the crystals exhibited sharp luminescence lines at 380, 420, 440, 460, 470, 490, 550, 590, and 620 nm. According to previous reports, these peaks were attributed to the 4f-4f transitions of Tb^{3+} [19,38–41]. The 0.3 and 1% Tb-doped crystals showed a broad emission band around 440 nm as well. The broad emission band was considered due to the oxygen and cation vacancies of the host material [42,43]. The PL QYs of the crystals upon 250 nm excitation are summarized in Table 1. The highest QY was obtained from the 3% Tb-doped crystal among the present crystals, and concentration quenching occurred in the 5% Tb-doped crystal. Our device for QY can allow only excitation wavelengths longer than 250 nm. Therefore, if the crystals are excited by 230 nm, which is a suitable excitation wavelength, a higher QY will be expected.

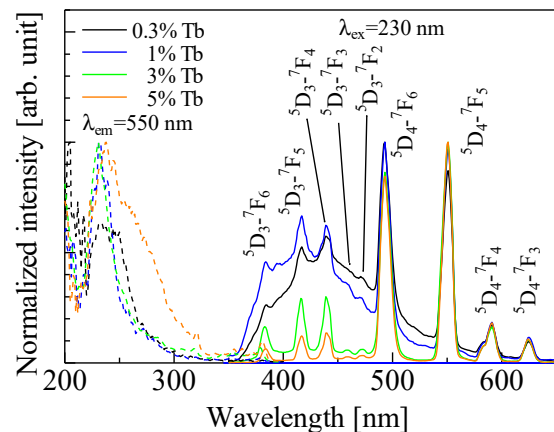


Figure 4. PL excitation (dashed line) and emission (solid line) spectra of Tb-doped MgGa_2O_4 .

Table 1. PL QY and decay time constants of the crystals.

| Sample | QY at 250 nm (%) | τ (μs) |
|---------|------------------|--------------------------|
| 0.3% Tb | 5.0 | 856 |
| 1% Tb | 6.5 | 627 |
| 3% Tb | 10.7 | 703 |
| 5% Tb | 4.4 | 877 |

Figure 5 shows the PL decay curves of the crystals. Obtained decay time constants are summarized in Table 1 as well as QY. Here, the excitation wavelength was set to 228 nm by using an optical filter, and the monitoring wavelength was 550 nm. All the decay curves were approximated with a single exponential decay function, and the obtained decay time constants were 627–877 μ s. These values are typical for the 4f-4f transitions of Tb^{3+} [44–46].

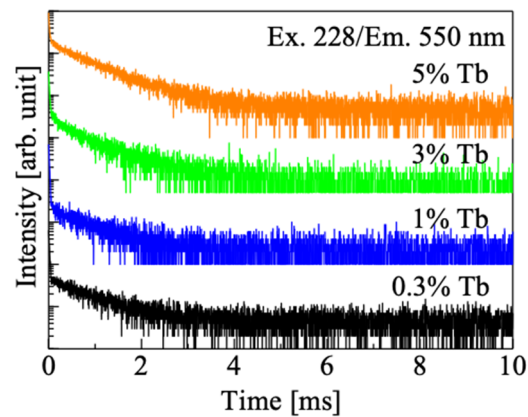


Figure 5. PL decay curves of Tb-doped $MgGa_2O_4$.

Figure 6 shows the TSL glow curves of the crystals after X-ray irradiation of 100 mGy. All the crystals exhibited a peak around 90 $^{\circ}C$. The peak was also observed in powder and ceramic forms of $MgGa_2O_4$, and the origin was related to intrinsic antisite defects due to cation inversion [27,47]. Thus, antisite defects were useful as the trapping center, even in a single crystal form. Luminescence intensity followed PL QY, and the highest luminescence intensity was confirmed from the 3% Tb-doped crystal. The crystals were stable when heated at 490 $^{\circ}C$. Therefore, the crystals can be used stably as a TSL dosimetric material.

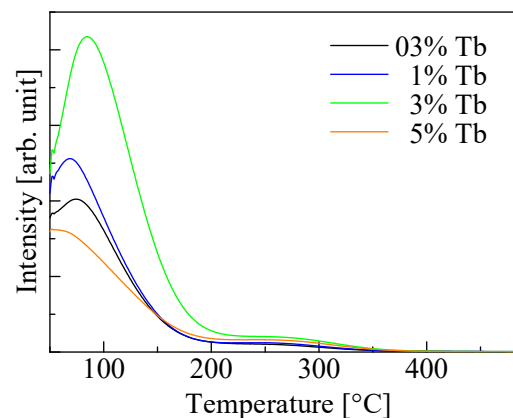


Figure 6. TSL glow curves of Tb-doped $MgGa_2O_4$ after X-ray irradiation of 100 mGy.

To clarify the luminescence origin of the crystals in TSL, TSL spectra were measured. Here, the result of the 3% Tb-doped crystal, which exhibited the highest TSL intensity, is shown as the representative since all the crystals showed the same trend. Figure 7a indicates the TSL spectra of the 3% Tb-doped crystal stimulated by 90 and 150 $^{\circ}C$ after X-ray irradiation with 10 Gy. Figure 7b shows an enlarged view in the range of 350 to 500 nm. The emission peaks due to 4f-4f transitions of Tb^{3+} were observed from 380 to 620 nm, as well as PL. On the other hand, there was no broad emission band due to oxygen and cation vacancies, unlike in PL. Therefore, Tb^{3+} played a major role in the TSL luminescence center, and oxygen and cation vacancies probably acted as trapping centers in TSL together with antisite defects. In addition, as shown in Figure 7b, the emission peaks related to the 5D_3 level vanished over 150 $^{\circ}C$ because of thermal quenching [48]. In addition, TSL intensity in

Figure 6 might have been underestimated, especially above 150 °C, because the apparatus for TSL glow curves had an optical filter that cut photons with a wavelength longer than 520 nm.

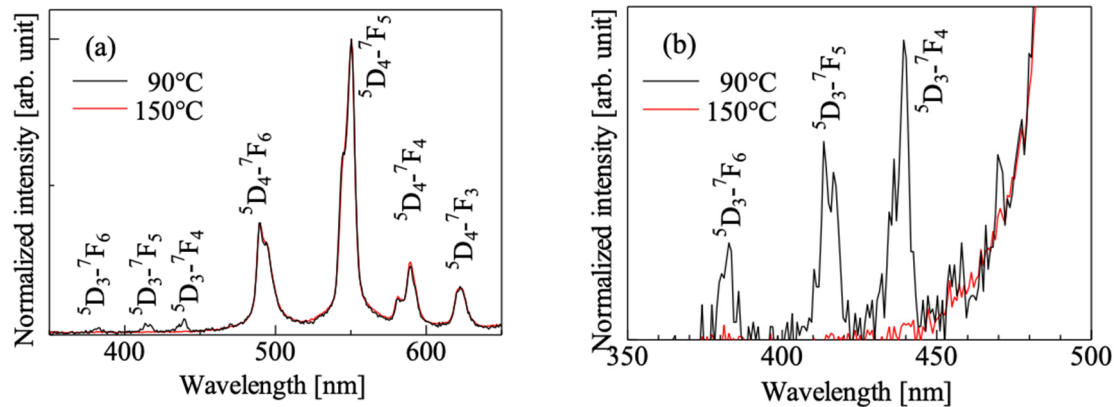


Figure 7. (a) TSL spectra of 3% Tb-doped MgGa_2O_4 stimulated by 90 and 150 °C after X-ray irradiation with 10 Gy; (b) shows enlarged view between 350 and 500 nm.

Figure 8 presents the TSL dose response functions of the crystals. The intensity was defined as the peak height at 90 °C. The minimum detectable dose of all the crystals was 0.01 mGy, which was comparable with those of some commercial dosimeters, although fading of the samples may be strong [49]. In addition, 0.01 mGy was the lowest dose that could be tested in our setup, and the signal intensity saturated when the irradiated dose exceeded 100 mGy for the 3% Tb-doped crystal and 300 mGy for the other crystals. Therefore, the crystals may be used in a wider dose range.

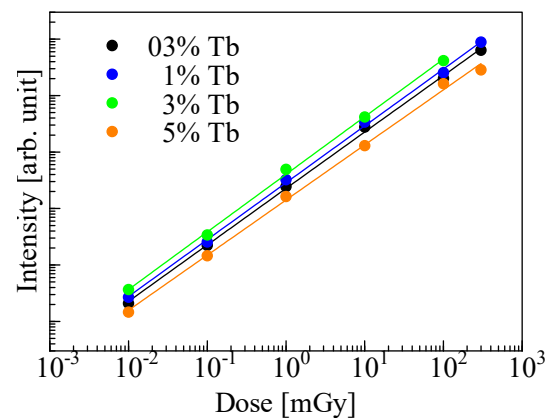


Figure 8. TSL dose response functions of Tb-doped MgGa_2O_4 .

Figure 9 shows the results of the X-ray imaging test of the 1% Tb-doped crystal taken by using TSL. Here, the clearest image was obtained from the 1% Tb-doped crystal among the present crystals because of the fewest cracks. Figure 9a,b indicates the obtained image and intensity profiles of each line pattern, respectively. As shown in Figure 9a, luminescence was observed only in the area irradiated by X-rays, while luminescence was not observed in the rest since X-rays were blocked by the Pb substrate. From Figure 9b, the line patterns were well resolved, and the spatial resolution of the 1% Tb-doped crystal was 8.90 LP/mm (56.2 μm). This result indicates that a Tb-doped MgGa_2O_4 single crystal can be applied to 2D dosimetry (TL imaging plate) as well. In addition, the 3% Tb-doped crystal, which showed the highest luminescence intensity, can demonstrate higher spatial resolution than a 1% Tb-doped crystal if a crystal with no cracks is grown.

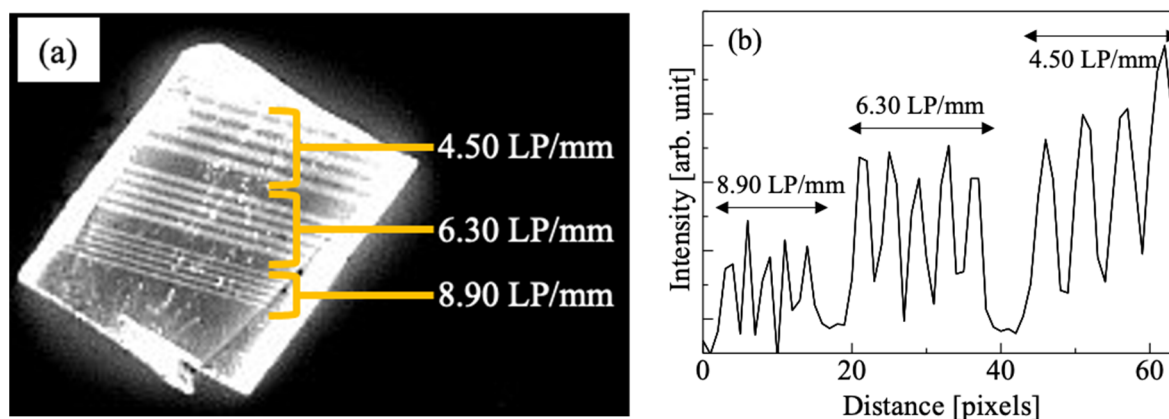


Figure 9. Results of X-ray imaging test of 1% Tb-doped MgGa_2O_4 taken by TSL: (a) obtained image; (b) intensity profiles of each line pattern.

4. Conclusion

MgGa_2O_4 single crystals doped with various concentrations of Tb were synthesized by the FZ method. The XRD patterns showed a single phase of MgGa_2O_4 . In PL, Tb^{3+} and oxygen and cation vacancies worked as luminescence centers. The highest QY value was obtained in the 3% Tb-doped crystal. In TSL, Tb^{3+} acted as a luminescence center, as well as PL; on the other hand, oxygen and cation vacancies played the role of trapping centers, unlike PL. The 3% Tb-doped crystal exhibited the highest TSL intensity, as well as QY. The minimum detectable dose of the crystals was 0.01 mGy, which was comparable with some commercial dosimeters. In the X-ray imaging test using TSL, the spatial resolution of the 1% Tb-doped crystal was estimated to be 8.90 LP/mm (56.2 μm). Although the TL glow peak at 90 $^\circ\text{C}$ was unstable owing to fading, these results indicate that Tb-doped MgGa_2O_4 single crystals are applicable to personal and environmental dosimetry and X-ray imaging.

Author Contributions: Conceptualization, Y.T.; methodology, Y.T.; validation, K.N., T.K., D.N. and N.K.; formal analysis, Y.T., S.H., T.K. and T.Y.; investigation, Y.T. and S.H.; resources, T.Y.; data curation, Y.T.; writing-original draft preparation, Y.T.; writing-review and editing, Y.T. and T.Y.; visualization, Y.T.; supervision, K.N., T.K., D.N., N.K. and T.Y.; funding acquisition, T.K., D.N., N.K. and T.Y. All authors have read and agreed to the published version of the manuscript.

Funding: This work was supported by Grant-in-Aid for Scientific Research A (22H00309), Scientific Research B (21H03733, 21H03736, 22H02939, and 22H03872), and Challenging Exploratory Research (22K18997) from the Japan Society for the Promotion of Science. The Foundation from the Cooperative Research Project of the Research Center for Biomedical Engineering, the Nippon Sheet Glass Foundation, the Terumo Life Science Foundation, the Iwatani Naoji Foundation, and the Konica Minolta Science and Technology Foundation are also acknowledged.

Institutional Review Board Statement: Not applicable.

Informed Consent Statement: Not applicable.

Data Availability Statement: Data of the results presented in this article are not publicly available.

Conflicts of Interest: The authors declare no conflict of interest.

References

1. Yanagida, T.; Okada, G.; Kawaguchi, N. Ionizing-Radiation-Induced Storage-Luminescence for Dosimetric Applications. *J. Lumin.* **2019**, *207*, 14–21. [[CrossRef](#)]
2. Bhatt, B.C.; Kulkarni, M.S. Worldwide Status of Personnel Monitoring Using Thermoluminescent (TL), Optically Stimulated Luminescent (OSL) and Radiophotoluminescent (RPL) Dosimeters. *Int. J. Lumin. Appl.* **2013**, *3*, 6–10.
3. Viamonte, A.; da Rosa, L.A.R.; Buckley, L.A.; Cherpak, A.; Cygler, J.E. Radiotherapy Dosimetry Using a Commercial OSL System. *Med. Phys.* **2008**, *35*, 1261–1266. [[CrossRef](#)] [[PubMed](#)]
4. Watanabe, K.; Yamazaki, A.; Nakahashi, K.; Miyamae, H.; Uritani, A.; Ariga, E. Development of a Micro-Size Dosimeter Using an Optical Fiber Probe Based on Photostimulable Phosphorescence. *Radiat. Meas.* **2013**, *55*, 64–67. [[CrossRef](#)]

5. Nanto, H.; Nishimura, A.; Kuroda, M.; Takei, Y.; Nakano, Y.; Shoji, T.; Yanagita, T.; Kasai, S. X-ray Imaging Plate Using CsBr:Eu Phosphors for Computed Radiography. *Nucl. Instrum. Methods Phys. Res. Sect. A* **2007**, *580*, 278–281. [[CrossRef](#)]
6. McKeever, S.W.S. Optically Stimulated Luminescence: A Brief Overview. *Radiat. Meas.* **2011**, *46*, 1336–1341. [[CrossRef](#)]
7. Akça, S.; Portakal, Z.G.; Dogan, T.; Kucuk, N.; Canimoglu, A.; Topaksu, M.; Can, N. Thermoluminescence Properties of Tb Doped Mg₂SiO₄ after Beta Irradiation. *Nucl. Instrum. Methods Phys. Res. Sect. B* **2019**, *458*, 12–20. [[CrossRef](#)]
8. Bos, A.J.J.; Dielhof, J.B. The Analysis of Thermoluminescent Glow Peaks in CaF₂:Tm (TLD-300). *Radiat. Prot. Dosim.* **1991**, *37*, 231–239. [[CrossRef](#)]
9. Fiksel, G.; Marshall, F.J.; Mileham, C.; Stoeckl, C. Note: Spatial Resolution of Fuji BAS-TR and BAS-SR Imaging Plates. *Rev. Sci. Instrum.* **2012**, *83*, 086103. [[CrossRef](#)]
10. Zhao, Y.; Zhou, Y.; Jiang, Y.; Zhou, W.; Finch, A.A.; Townsend, P.D.; Wang, Y. Ion Size Effects on Thermoluminescence of Terbium and Europium Doped Magnesium Orthosilicate. *J. Mater. Res.* **2015**, *30*, 3443–3452. [[CrossRef](#)]
11. Yanagisawa, S.; Shinsho, K.; Inoue, M.; Koba, Y.; Matsumoto, K.; Ushiba, H.; Andoh, T. Applicability of Two-Dimensional Thermoluminescence Slab Dosimeter Based on Al₂O₃:Cr for the Quality Assurance of Robotic Radiosurgery. *Radiat. Meas.* **2017**, *106*, 326–330. [[CrossRef](#)]
12. Takebuchi, Y.; Kato, T.; Nakauchi, D.; Kawaguchi, N.; Yanagida, T. Dosimetric Properties of Dy-Doped LiCaPO₄. *Optik* **2022**, *260*, 169079. [[CrossRef](#)]
13. Kato, T.; Nakauchi, D.; Kawaguchi, N.; Yanagida, T. TSL and OSL Properties of Cu-Doped CaF₂ Ceramics Prepared by Spark Plasma Sintering. *Sens. Mater.* **2022**, *34*, 653. [[CrossRef](#)]
14. Oh, R.; Yanagisawa, S.; Tanaka, H.; Takata, T.; Wakabayashi, G.; Tanaka, M.; Sugioka, N.; Koba, Y.; Shinsho, K. Thermal Neutron Measurements Using Thermoluminescence Phosphor Cr-Doped Al₂O₃ and Cd Neutron Converter. *Sens. Mater.* **2021**, *33*, 2129. [[CrossRef](#)]
15. Schmocker, U.; Boesch, H.R.; Waldner, F. A Direct Determination of Cation Disorder in MgAl₂O₄ Spinel by ESR. *Phys. Lett. A* **1972**, *40*, 237–238. [[CrossRef](#)]
16. Gritsyna, V.T.; Kazarinov, Y.G.; Kobayakov, V.A.; Sickafus, K.E. Defects and Radiation Induced Electronic Processes in Magnesium Aluminate Spinel of Different Compositions. *Radiat. Eff. Defects Solids* **2002**, *157*, 659–663. [[CrossRef](#)]
17. Pathak, N.; Ghosh, P.S.; Gupta, S.K.; Mukherjee, S.; Kadam, R.M.; Arya, A. An Insight into the Various Defects-Induced Emission in MgAl₂O₄ and Their Tunability with Phase Behavior: Combined Experimental and Theoretical Approach. *J. Phys. Chem. C* **2016**, *120*, 4016–4031. [[CrossRef](#)]
18. Khan, K.; Satapathy, K.K.; Mishra, G.C. Thermoluminescence Characterization of MAl₂O₄ (M=Ba, Ca, Mg) Phosphors Activated with Dy³⁺. *Int. J. Lumin. Appl.* **2015**, *5*, 26–28.
19. Takebuchi, Y.; Fukushima, H.; Kato, T.; Nakauchi, D.; Kawaguchi, N.; Yanagida, T. Dosimetric Properties of Tb-Doped MgAl₂O₄ Single Crystals. *Jpn. J. Appl. Phys.* **2020**, *59*, 052007. [[CrossRef](#)]
20. Takebuchi, Y.; Fukushima, H.; Kato, T.; Nakauchi, D.; Kawaguchi, N.; Yanagida, T. Thermally Stimulated Luminescence Properties of Dy-Doped MgAl₂O₄ Single Crystals. *Optik* **2021**, *231*, 166498. [[CrossRef](#)]
21. Takebuchi, Y.; Koshimizu, M.; Kato, T.; Nakauchi, D.; Kawaguchi, N.; Yanagida, T. Effect of Tm Doping on Photoluminescence, Scintillation, and Thermally Stimulated Luminescence Properties of MgAl₂O₄ Single Crystals. *J. Lumin.* **2022**, *251*, 119247. [[CrossRef](#)]
22. Takebuchi, Y.; Fukushima, H.; Nakauchi, D.; Kato, T.; Kawaguchi, N.; Yanagida, T. Scintillation and Dosimetric Properties of Ce-Doped MgAl₂O₄ Single Crystals. *J. Lumin.* **2020**, *223*, 117139. [[CrossRef](#)]
23. Bos, A.J.J. Theory of Thermoluminescence. *Radiat. Meas.* **2006**, *41*, S45–S56. [[CrossRef](#)]
24. Galazka, Z.; Klimm, D.; Irmscher, K.; Uecker, R.; Pietsch, M.; Bertram, R.; Naumann, M.; Albrecht, M.; Kwasniewski, A.; Schewski, R.; et al. MgGa₂O₄ as a New Wide Bandgap Transparent Semiconducting Oxide: Growth and Properties of Bulk Single Crystals. *Phys. Status Solidi* **2015**, *212*, 1455–1460. [[CrossRef](#)]
25. Hosseini, S.M. Structural, Electronic and Optical Properties of Spinel MgAl₂O₄ Oxide. *Phys. Status Solidi* **2008**, *245*, 2800–2807. [[CrossRef](#)]
26. Luchechko, A.; Zhydashkevskyy, Y.; Maraba, D.; Bulur, E.; Ubizskii, S.; Kravets, O. TL and OSL Properties of Mn²⁺-Doped MgGa₂O₄ Phosphor. *Opt. Mater.* **2018**, *78*, 502–507. [[CrossRef](#)]
27. Mlotswa, D.V.; Noto, L.L.; Mofokeng, S.J.; Obodo, K.O.; Orante-Barrón, V.R.; Mothudi, B.M. Luminescence Dynamics of MgGa₂O₄ Prepared by Solution Combustion Synthesis. *Opt. Mater.* **2020**, *109*, 110134. [[CrossRef](#)]
28. Takebuchi, Y.; Fukushima, H.; Kato, T.; Nakauchi, D.; Kawaguchi, N.; Yanagida, T. Optical, Scintillation, and Dosimetric Properties of Mn-Doped MgAl₂O₄ Single Crystals. *J. Mater. Sci. Mater. Electron.* **2020**, *31*, 8240–8247. [[CrossRef](#)]
29. Yanagida, T.; Fujimoto, Y.; Kawaguchi, N.; Yanagida, S. Dosimeter Properties of AlN. *J. Ceram. Soc. Jpn.* **2013**, *121*, 988–991. [[CrossRef](#)]
30. Okada, G.; Kato, T.; Nakauchi, D.; Fukuda, K.; Yanagida, T. Photochromism and Thermally and Optically Stimulated Luminescences of AlN Ceramic Plate for UV Sensing. *Sens. Mater.* **2016**, *28*, 897. [[CrossRef](#)]
31. Okada, G.; Fukuda, K.; Kasap, S.; Yanagida, T. Aluminum Nitride Ceramic as an Optically Stimulable Luminescence Dosimeter Plate. *Photonics* **2016**, *3*, 23. [[CrossRef](#)]
32. Liu, H.; Yu, L.; Li, F. Photoluminescent Properties of Eu³⁺ and Dy³⁺ Ions Doped MgGa₂O₄ Phosphors. *J. Phys. Chem. Solids* **2013**, *74*, 196–199. [[CrossRef](#)]

33. Zhang, G.; Goldstein, A.; Wu, Y. Novel Transparent MgGa_2O_4 and Ni^{2+} -Doped MgGa_2O_4 Ceramics. *J. Adv. Ceram.* **2022**, *11*, 470–481. [[CrossRef](#)]
34. Basavaraju, N.; Sharma, S.; Bessière, A.; Viana, B.; Gourier, D.; Priolkar, K.R. Red Persistent Luminescence in MgGa_2O_4 : Cr^{3+} ; a New Phosphor for in Vivo Imaging. *J. Phys. D. Appl. Phys.* **2013**, *46*, 375401. [[CrossRef](#)]
35. Ichiba, K.; Takebuchi, Y.; Kimura, H.; Kato, T.; Nakauchi, D.; Kawaguchi, N.; Yanagida, T. Photoluminescence, Scintillation, and Dosimetric Properties of Tb-Doped Mg_2SiO_4 Single Crystals. *J. Mater. Sci. Mater. Electron.* **2022**, *33*, 13634–13641. [[CrossRef](#)]
36. Yang, H.; Shi, J.; Gong, M.; Cheah, K.W. Synthesis and Photoluminescence of Eu^{3+} - or Tb^{3+} -Doped Mg_2SiO_4 Nanoparticles Prepared by a Combined Novel Approach. *J. Lumin.* **2006**, *118*, 257–264. [[CrossRef](#)]
37. Ichiba, K.; Takebuchi, Y.; Kimura, H.; Kato, T.; Shiratori, D.; Nakauchi, D.; Kawaguchi, N.; Yanagida, T. Synthesis of Tb-Doped SiO_2 Glasses by Spark Plasma Sintering Method and Evaluation of Photoluminescence and Thermally Stimulated Luminescence Properties. *Radiat. Phys. Chem.* **2023**, *202*, 110515. [[CrossRef](#)]
38. Nakauchi, D.; Kato, T.; Kawaguchi, N.; Yanagida, T. Photoluminescence and Scintillation Properties of $\text{Tb}:\text{GdTaO}_4$ Crystals. *Sens. Mater.* **2021**, *33*, 2203. [[CrossRef](#)]
39. Nakagawa, H.; Ebisu, K.; Zhang, M.; Kitaura, M. Luminescence Properties and Afterglow in Spinel Crystals Doped with Trivalent Tb Ions. *J. Lumin.* **2003**, *102–103*, 590–596. [[CrossRef](#)]
40. Ratnam, B.V.; Jayasimhadri, M.; Bhaskar Kumar, G.; Jang, K.; Kim, S.S.; Lee, Y.I.; Lim, J.M.; Shin, D.S.; Song, T.K. Synthesis and Luminescent Features of NaCaPO_4 : Tb^{3+} Green Phosphor for near UV-Based LEDs. *J. Alloy. Compd.* **2013**, *564*, 100–104. [[CrossRef](#)]
41. Nakauchi, D.; Fukushima, H.; Kato, T.; Kawaguchi, N.; Yanagida, T. Photoluminescence and Scintillation Properties of Ce-, Pr-, and Tb-Doped $(\text{Gd},\text{Lu})_2\text{Hf}_2\text{O}_7$ Crystals. *Sens. Mater.* **2022**, *34*, 611. [[CrossRef](#)]
42. Jiang, B.; Chi, F.; Wei, X.; Chen, Y.; Yin, M. A Self-Activated MgGa_2O_4 for Persistent Luminescence Phosphor. *J. Appl. Phys.* **2018**, *124*, 063101. [[CrossRef](#)]
43. Liu, Z.; Hu, P.; Jing, X.; Wang, L. Luminescence of Native Defects in MgGa_2O_4 . *J. Electrochem. Soc.* **2009**, *156*, H43. [[CrossRef](#)]
44. Liu, F.S.; Liu, Q.L.; Liang, J.K.; Luo, J.; Yang, L.T.; Song, G.B.; Zhang, Y.; Wang, L.X.; Yao, J.N.; Rao, G.H. Crystal Structure and Photoluminescence of Tb^{3+} Doped Y_3GaO_6 . *J. Alloy. Compd.* **2006**, *425*, 278–283. [[CrossRef](#)]
45. Dahiya, H.; Dalal, M.; Dalal, J.; Taxak, V.B.; Khatkar, S.P.; Kumar, D. Synthesis and Luminescent Properties of Tb^{3+} Doped $\text{BaLa}_2\text{ZnO}_5$ Nanoparticles. *Mater. Res. Bull.* **2018**, *99*, 86–92. [[CrossRef](#)]
46. Liao, J.; Qiu, B.; Lai, H. Synthesis and Luminescence Properties of $\text{Tb}^{3+}:\text{NaGd}(\text{WO}_4)_2$ Novel Green Phosphors. *J. Lumin.* **2009**, *129*, 668–671. [[CrossRef](#)]
47. Matsui, H.; Xu, C.-N.; Akiyama, M.; Watanabe, T. Strong Mechanoluminescence from UV-Irradiated Spinel of ZnGa_2O_4 :Mn and MgGa_2O_4 :Mn. *Jpn. J. Appl. Phys.* **2000**, *39*, 6582–6586. [[CrossRef](#)]
48. Boruc, Z.; Fetlinski, B.; Kaczkan, M.; Turczynski, S.; Pawlak, D.; Malinowski, M. Temperature and Concentration Quenching of Tb^{3+} Emissions in $\text{Y}_4\text{Al}_2\text{O}_9$ Crystals. *J. Alloy. Compd.* **2012**, *532*, 92–97. [[CrossRef](#)]
49. Bhatt, B.C. Thermoluminescence, Optically Stimulated Luminescence and Radiophotoluminescence Dosimetry: An Overall Perspective. *Radiat. Prot. Environ.* **2011**, *34*, 6–16.